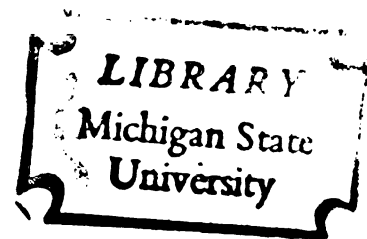




109
426
THS






This is to certify that the
thesis entitled
RESONANCE RAMAN STUDIES
OF CYCLIC AND LINEAR POLYENES

presented by
DAVID ARTHUR GOBELI

has been accepted towards fulfillment
of the requirements for
M.S. degree in Chemistry


Major professor

Date 10 August 1949



OVERDUE FINES:

25¢ per day per item

RETURNING LIBRARY MATERIALS:

Place in book return to remove
charge from circulation records

--	--

RESONANCE RAMAN STUDIES OF CYCLIC AND
LINEAR POLYENES

By

David Arthur Gobell

A THESIS

Submitted to

Michigan State University

in partial fulfillment of the requirements

for the degree of

MASTER OF SCIENCE

Department of Chemistry

1979

ABSTRACT

RESONANCE RAMAN STUDIES OF CYCLIC AND LINEAR POLYENES

By

David Arthur Gobeli

Raman excitation profiles were obtained for oxidized heme-a and β -carotene, compounds of both theoretical and biological interest. The tunable excitation radiation was provided by a continuous wave dye laser.

The excitation profile of heme-a was taken at selected wavelengths in the visible region of the spectrum in order to facilitate the characterization of two electronic transitions, with absorption peaks at 590 and 545 nm, for which the assignments are in dispute. The results suggest that the absorptions correspond to a weak π - π^* transition of the cyclic polyene chromophore of the porphyrin ring and its vibronic sideband.

The excitation profile of β -carotene was obtained at closely spaced excitation wavelengths in the preresonance region of the absorption spectrum. Interferences in the

preresonance Raman excitation profile indicate the presence of a low-lying symmetry-forbidden excited electronic state in this linear polyene.

TABLE OF CONTENTS

Chapter	Page
LIST OF TABLES.	111
LIST OF FIGURES	iv
CHAPTER I INTRODUCTION	1
CHAPTER II EXPERIMENTAL	3
CHAPTER III HEME-A	12
Theory.	15
Experimental.	23
Results	24
Suggestions for Further Work.	27
CHAPTER IV β -CAROTENE	28
Theory.	29
Experimental.	32
Results	33
Suggestions for Further Work.	33
APPENDIX - Preparation of Dye Solutions.	36
REFERENCES.	37

LIST OF TABLES

Table		Page
1	Laser Dyes Used, Effective Tuning Range and Typical Output Power	6
2	Raman Intensities of Oxidized Heme-a.	26

LIST OF FIGURES

Figure		Page
1	Dye Laser Configuration.	5
2	Correct Image From the Folding Mirror	9
3	Oxidized Heme-a.	13
4	Visible Spectrum of Oxidized Heme-a (bis-N-methyl imidazole).	13
5	Resonance Raman Spectra of Oxidized Heme-a.	25
6	β -Carotene	29
7	Raman Excitation Profile of β -Carotene in Preresonance Region	34

CHAPTER 1

INTRODUCTION

With the development of the dye laser as a source of continuously tunable monochromatic radiation, the use of resonance Raman spectroscopy as a tool for studying problems of both theoretical and biological importance has grown considerably. The advantages are twofold: the resonance Raman effect selectively enhances the vibrations of the electronic chromophore of interest relative to any others, and because of the corresponding increase in sensitivity, many otherwise inaccessible compounds - notably those of biological significance, which don't occur naturally in high enough concentration to be observable by the normal Raman effect - may be studied.¹ In addition, from a plot of the intensity of specific features against the Raman excitation energy information can be gained relative to the electronic transition of interest. This is known as the Raman excitation profile.

Moreover, if one studies the Raman excitation profile in the "preresonance" region of the electronic spectrum, an area on the tailing edge of a visible absorption band, electronic states not ordinarily detected by conventional

spectroscopic techniques may be observed.² This form of the excitation profile is useful in detecting low-lying energy states not accessible by electric dipole absorption from the ground state.

In this thesis two polyenes, each of both biological and theoretical interest, will be studied. The first, heme-a, is a cyclic polyene found in the majority of living organisms; from its resonance Raman excitation profiles assignments will be made as to the nature of the electronic transitions in the visible region of its spectrum. For the second compound, β -carotene, the Raman excitation profile in the "preresonance" region of the electronic spectrum will be examined; several vibronic states which are not observed by conventional visible absorption techniques, due to their forbidden nature, will be characterized.

CHAPTER 2

EXPERIMENTAL

A Raman excitation profile is simply a plot of the scattering intensity of a particular feature plotted against the exciting line wavenumber at constant incident power. Since maintaining constant output power from a dye laser when changing exciting wavelengths and dyes is difficult, a modification of this technique is necessary in order to take this fluctuation into account. This is accomplished by measuring the scattering intensity of the feature of interest with respect to some internal standard such as a solvent peak, for which the intensity is invariant over the tuning range of interest.

The equipment necessary to obtain Raman excitation profiles includes a continuously tunable light source in addition to the optics, monochromator and detection electronics normally required to perform Raman spectroscopy. Laser light whose output wavelength can be varied continuously over a wide range can be attained from a continuous wave (cw) dye laser. From a tunable dye laser, relatively high-power radiation can be attained for use as a monochromatic Raman excitation source in wavelength regions

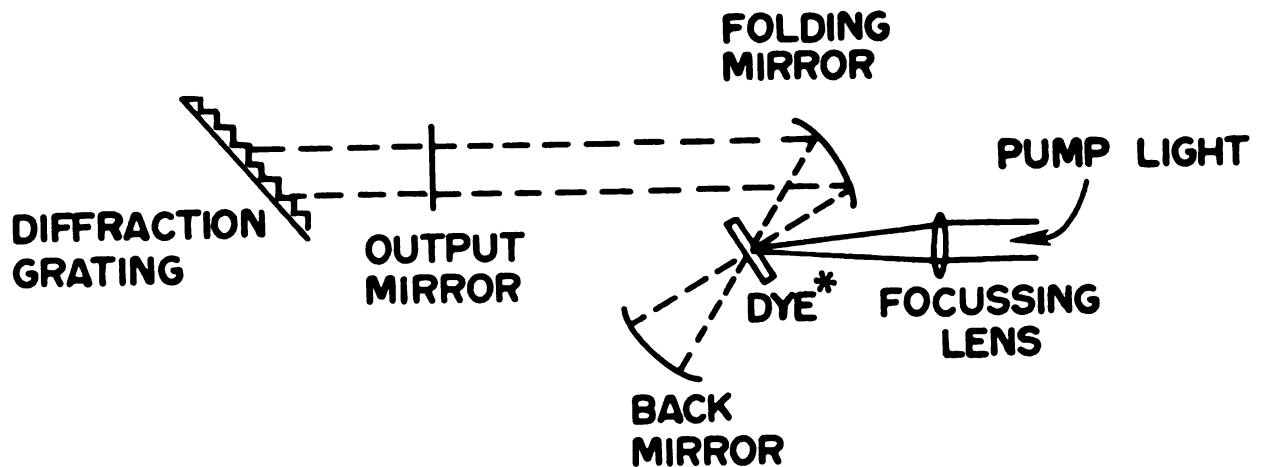
inaccessible by conventional fixed-frequency high-powered gas lasers, such as the argon or krypton ion visible lasers.

Although the cw dye laser in this laboratory is similar to commercially available models, it possesses several unique features, so its operation will be detailed.³

High intensity pumping radiation, typically the all-lines output from either an argon or krypton ion laser, is necessary in order to produce lasing within a dye solution. The pump used in this experiment is a Spectra-Physics Model 164 argon ion laser producing typically 4-5 watts of output power when used in the "all-lines" mode. This output is focussed onto a flowing jet stream of laser dye which is continuously circulated in order to prevent the rapid heating, and subsequent rapid degradation of the dye solution, which would otherwise be caused by utilizing a stationary dye cell in the focus of the pumping laser. In addition, the dye solution is cooled, usually with dry ice.

A basic three-mirror cavity is constructed around the dye jet as shown in Figure 1.³

The cavity consists of front, back and folding mirrors obtained from commercial sources. This configuration is used in preference to a standard two-mirror cavity in order to compensate for the astigmatism caused by having the dye jet at Brewster's angle with respect to the



***Flow of dye solution
is perpendicular to page**

Figure 1. Dye Laser Configuration.

incident pumping radiation, and to eliminate the need of using a focussing mirror instead of the focussing lens which is employed in the three-mirror cavity. A diffraction grating which is placed after the output mirror is used to tune the output of the dye laser and provides a typical bandwidth of 0.1 nm. A Spectra-Physics Model 376 dye circulator and nozzle are used to produce the dye jet stream. In order to maintain a uniform dye film through the active region of the cavity it is necessary to use a viscous solvent for the dye. For the dyes used

in this work the solvent chosen was ethylene glycol or an ethylene glycol/benzyl alcohol mixture. Table 1 lists the dyes used and the wavelength region over which each could be effectively tuned. With the exception of

Table 1. Laser Dyes Used, Effective Tuning Ranges and Typical Output Power.

Dye	Tuning Range	Typical Output Power
Coumarin-6	522-552 nm	60-120 mw
Disodium fluorescein	540-575 nm	120-400 mw
Rhodamine-6G	570-640 nm	300-600 mw

Rhodamine-6G, it is necessary to add varying amounts of cyclooctatetraene (COT) to the dye solution; COT serves as a triplet quencher for the dye and thus enables lasing. The exact preparation method for each dye solution is outlined in the Appendix.

The tuned laser radiation is collected off of the grating and is used directly by way of completely reflecting mirrors which serve as beam directors. This method is not quite as convenient as that outlined in R. J. Thrash's thesis,³ where a beamsplitter was employed within the cavity to eliminate the need for adjusting the beam directing optics as the excitation wavelength is changed.

However, it is superior in that the usable output power is much higher. The power available with this configuration ranged typically from 100-800 mw vs. 5-40 mw attained by Thrash. This increase of more than an order of magnitude of usable output provides a substantial increase in the signal-to-noise ratio in the Raman spectra obtained. The output power from all dyes remained stable for many hours.

Since the cw dye laser used in these experiments is "home-made" and easily disassembled, the cavity alignment procedure will be outlined in detail. The optical mounting equipment used in this dye laser is designed for easy interchange of mirrors. This is necessary because each specific tuning region requires specifically coated optical substrates which optimize the output power for the particular dye being used. The back mirrors used (Coherent Radiation) have a focal length of 50 mm and the folding mirrors have a focal length of 75 mm. All are 0.5 inch in diameter and are coated to provide maximum reflectivity at the lasing wavelengths of the particular dye being circulated. The output mirror, sometimes referred to as the transmitter, or output coupler, is flat and is usually 95-98% reflecting, depending on the mirror being used and the wavelength at which the laser is operating. The focussing lens used for the argon ion beam is an achromat with a focal length of 22 mm and a

diameter of 10 mm. A step-by-step procedure for the alignment procedure follows.

Step 1. With the argon ion laser operating at minimal power, position the output so that it strikes the flowing dye jet about 0.5 cm or so from the nozzle at an approximate right angle. All other optical elements should be removed at this step.

Step 2. Rotate the nozzle of the dye circulator so that the right angle between the argon ion beam and the direction of the flow is maintained, but the reflected laser intensity is minimized. This should be attained at Brewster's angle.

Step 3. Insert the achromatic lens and bring the argon ion beam into sharp focus onto the dye jet. The reflection, which will be observed on the ceiling, should now look like two round spots which may or may not be coincident. If the argon ion beam is improperly focussed, the spots may not be round.

Step 4. Insert the output mirror about 1 foot from the dye jet and position it vertically so that its center is approximately coplanar with the dye jet and argon ion beam.

Step 5. Now insert the folding mirror in the dye cavity so that it is as close to the plane defined by the dye jet intersecting the argon ion beam as possible. Its approximate position will be directly above the

focussing lens. Now adjust the folding mirror so that the light from the dye jet is reflected onto the output mirror. Adjusting the distance of the folding mirror from the dye jet, either vertically or horizontally, will change the shape of the spot hitting the output mirror. Now adjust the output mirror so that the spot is reflected onto a card mounted on top of the argon ion laser. Then position the folding mirror so that the shape of the image is approximately the same as is shown in Figure 2.



Figure 2. Correct Image From the Folding Mirror.

Step 6. This is the most difficult step. The back mirror is now inserted so that its center is approximately colinear with the folding mirror and the active region of the dye jet. The light reflected from the back mirror must now be passed back through the active region of the dye jet (where the argon ion light is focussed) onto the folding mirror, then onto the output mirror, and then onto the card. Once this is done, adjust its position so that the image caused by this mirror is the same shape as the one from the folding mirror. Then superimpose

the two images.

Step 7. Now tilt the output mirror so that the two superimposed spots fall on the folding mirror. The dye laser should now lase. At this point however, the radiation is not tuned.

Step 8. To achieve tunability, the grating should be inserted close to the output mirror so that the first-order reflection of the dye laser output re-enters the system. Now a slight rotation of the vertical axis of the grating should tune the dye laser output.

Once the radiation is tuned, it can be directed into the sample compartment of the monochromator. The direction of the polarization of the dye laser light will be the same as the argon ion laser light. The light is focussed by way of bottom illumination so as to be parallel to the entrance slit of the monochromator. The scattered radiation is collected, passed through a polarization scrambler, and finally onto the entrance slit of a Spex-Ramalog double monochromator. The scattered radiation is detected using an RCA C31034A photomultiplier tube cooled by a Products for Research TE-104TS thermoelectric cooler, typically maintained at -20 degrees C to minimize the dark current. The phototube housing circuitry is designed to operate in either a dc or photon counting mode. If the Raman scattering is sufficiently strong, the system is kept in the dc mode, with between 1900 and 2000 volts

applied phototube voltage and 3.0×10^{-8} amp full scale output presentation on a chart recorder. For weakly scattering samples photon counting, usually with similar voltages and 3.0×10^4 cps full scale deflection, is employed.

CHAPTER 3

HEME-A

The heme-based proteins are a class of compounds of tremendous biological interest, of which hemoglobin and cytochrome are two important examples.⁴ They consist of an iron-porphyrin moiety either chemically bonded or electrostatically attached to a larger protein superstructure. It is the heme portion of the protein which gives rise to the absorption maxima in the visible region of the spectrum. Hence, by use of the resonance Raman effect, it is possible to gain information about the porphyrin portion of the protein, or as described in this thesis, the isolated metalloporphyrin.

Many organisms contain cytochrome oxidase, which is necessary to mitochondrial respiration. Heme-a is the protein bound porphyrin which gives rise to peaks in the visible spectrum of cytochrome oxidase. By isolating this compound and applying resonance Raman spectroscopy to it, well-founded assignments can be made of the particular electronic transition giving rise to each of the visible absorption peaks.

Oxidized heme-a, whose structure is shown in Figure 3

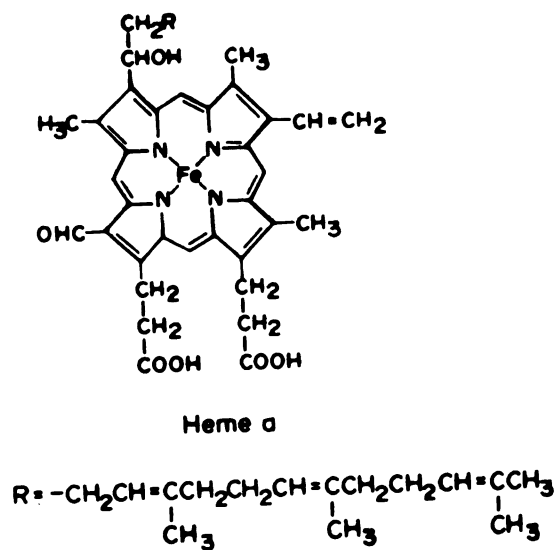


Figure 3. Oxidized Heme-a.

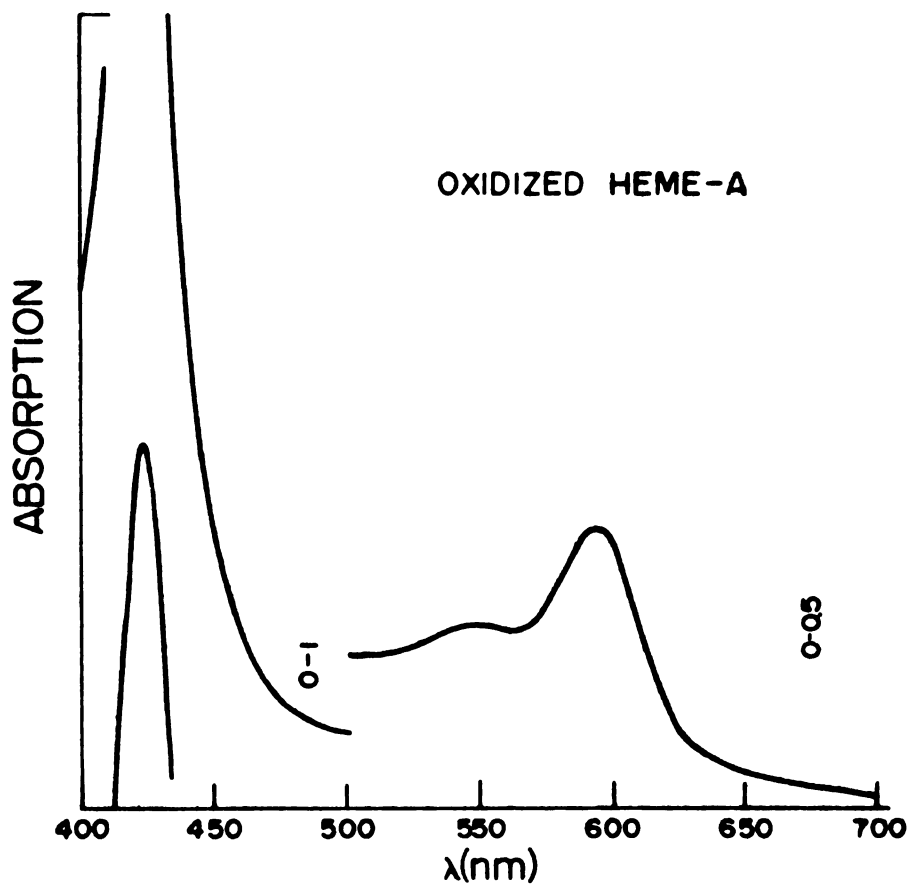


Figure 4. Visible Spectrum of Oxidized Heme-a (bis-N-methyl imidazole).

has a visible absorption spectrum consisting of three main features, as shown in Figure 4.

The most prominent absorption, an intense band centered at 422 nm with an extinction coefficient of about 10^5 is widely accepted as a strongly allowed $\pi-\pi^*$ transition in the 16-membered porphyrin ring. This feature is commonly referred to as either the B(0,0) or Soret band.⁵ Two much weaker features occur between 500 and 600 nm. Each has an extinction coefficient approximately one order of magnitude less than that of the Soret band. The assignment of the electronic transition corresponding to each of these bands is a subject of debate at the present time. One theory assigns the low energy band at 590 nm, based upon magnetic circular dichroism (MCD) studies, to a charge-transfer band between the porphyrin ring and a formyl substituent attached to it.⁶ The remaining feature at 545 nm is assigned to a forbidden $\pi-\pi^*$ transition.

The other prominent theory attributes the low energy feature at 590 nm to a symmetry-forbidden $\pi-\pi^*$ transition of the porphyrin ring, the remaining feature at 545 nm being assigned as a vibronic sideband of the feature at 590 nm. In this model the 590 nm is assigned as the α or Q(0,0) band, and the 545 nm feature is termed the β or Q(1,0) band.⁷

From Raman spectra obtained with excitation wavelengths corresponding to approximately 590 and 545 nm it can be

readily determined, by observing which vibrational features are enhanced, which assignment is consistent with resonance Raman scattering theory.

Theory

The connection between the excited state electronic wavefunction and the observed enhanced intensities in various ground state vibrational modes arises from the vibronic coupling terms in equations describing the resonance Raman effect. A brief discussion of the non-resonance Raman effect is given first and then modifications are made for resonance Raman scattering.⁸

For the transition $\bar{g} \rightarrow \bar{f}$, the Raman scattering intensity per molecule averaged over all angles is given by:

$$I_{\bar{g} \rightarrow \bar{f}} = \frac{2^3 \pi (\omega - \omega_K)}{9c^4} I_0 \sum_{\rho\sigma} |(\alpha_{\rho\sigma})_{\bar{g}, \bar{f}}|^2 \quad (1)$$

I_0 represents the intensity of the incident radiation, $\hbar\omega_K = E - E_{\bar{g}}$, $\alpha_{\rho\sigma}$ is known as the scattering tensor and is related by a multiplicative factor and the vector potential to the polarizability, and ω is the (angular) frequency of the incident radiation. $\alpha_{\rho\sigma}$ is given by the Kramers-Heisenberg dispersion formula:

$$\begin{aligned}
(\alpha_{\rho\sigma})_{\bar{g},\bar{f}} = & \frac{\sum_{\bar{I}} \frac{\langle \bar{g} | \hat{\mu}_\rho | \bar{I} \rangle \langle \bar{I} | \hat{\mu}_\sigma | \bar{f} \rangle}{E_{\bar{I}} - E_{\bar{g}} - \hbar\omega}}{1} \\
& + \frac{\langle \bar{g} | \hat{\mu}_\rho | \bar{I} \rangle \langle \bar{I} | \hat{\mu}_\sigma | \bar{f} \rangle}{E_{\bar{I}} - E_{\bar{g}} + \hbar\omega} \quad (2)
\end{aligned}$$

The index \bar{I} represents a summation over all intermediate states. It should be noted that far from resonance $E_{\bar{I}} - E_{\bar{g}} - \hbar\omega \gg 0$ and both terms in the equation will contribute to the intensity of scattered radiation.

When resonance is approached $E_{\bar{I}} - E_{\bar{g}} - \hbar\omega = 0$ and a modification must be made to prevent the denominator in the first term of the scattering tensor from becoming zero. This is accomplished by adding a damping factor $i\Gamma_{\bar{I}}$, which takes into account the finite lifetime of the excited state $|\bar{I}\rangle$. The scattering tensor now becomes:

$$\begin{aligned}
(\alpha_{\rho\sigma})_{\bar{g},\bar{f}} = & \frac{\sum_{\bar{I}} \frac{\langle \bar{g} | \hat{\mu}_\rho | \bar{I} \rangle \langle \bar{I} | \hat{\mu}_\sigma | \bar{f} \rangle}{E_{\bar{I}} - E_{\bar{g}} - \hbar\omega - i\Gamma_{\bar{I}}}}{1} \\
& + \frac{\langle \bar{g} | \hat{\mu}_\rho | \bar{I} \rangle \langle \bar{I} | \hat{\mu}_\sigma | \bar{f} \rangle}{E_{\bar{I}} - E_{\bar{g}} + \hbar\omega - i\Gamma_{\bar{I}}} \quad (3)
\end{aligned}$$

Assuming that the damping factor is small, when the system is near resonance the first term will completely dominate.

Thus under the condition of resonance:

$$(\alpha_{\rho\sigma})_{\bar{g},\bar{f}} = \frac{\sum_{\bar{i}} \frac{\langle \bar{g} | \hat{\mu}_{\rho} | \bar{i} \rangle \langle \bar{i} | \hat{\mu}_{\sigma} | \bar{f} \rangle}{E_{\bar{i}} - E_{\bar{g}} - \hbar\omega - i\Gamma_{\bar{i}}} \quad (4)$$

The terms $|\bar{g}\rangle$, $|\bar{i}\rangle$, and $|\bar{f}\rangle$ represent the total wavefunction of the system. Under most circumstances the Schrödinger equation cannot be solved in this form, and approximations must be introduced which separate the wavefunction into a product of vibrational and electronic terms.

Utilizing the Born-Oppenheimer approximation one can write the complete wavefunction as a product:

$$|\bar{g}\rangle = |g\rangle |n\rangle \quad (5)$$

The term $|g\rangle |n\rangle$ represents a product of a purely electronic term $|g\rangle$ with a purely vibrational term $|n\rangle$. Thus, each matrix element within the polarizability tensor can now be written as the product of strictly vibrational and electronic integrals; it is assumed that $\hat{\mu}_{\rho}$ operates only on the electronic coordinates. The polarizability tensor may now be represented as a product of electronic and vibrational wavefunctions:

$$\begin{aligned}
(\alpha_{\rho\sigma})^{gn;fn'} &= \sum_{iv} \frac{\langle g|\hat{\mu}_\sigma|i\rangle\langle i|\hat{\mu}_\rho|f\rangle\langle n|v\rangle\langle v|n'\rangle}{E^{iv}-E^{gn}-\hbar\omega-i\Gamma_{iv}} \\
&= \sum_{iv} \frac{M_{gi}^\sigma M_{if}^0 \langle n|v\rangle\langle v|n'\rangle}{E^{iv}-E^{gn}-\hbar\omega-i\Gamma_{iv}} \quad (6)
\end{aligned}$$

For the normal resonance Raman effect $|g\rangle$, the initial electronic state, will be the same as the final electronic state $|f\rangle$. Thus:

$$(\alpha_{\rho\sigma})^{gn,gn'} = \sum_{iv} \frac{M_{gi}^\sigma M_{ig}^0 \langle n|v\rangle\langle v|n'\rangle}{E^{iv}-E^{gn}-\hbar\omega-i\Gamma_{iv}} \quad (7)$$

The symbols M_{gi}^σ and M_{ig}^0 represent electronic transition dipoles and will be equal if both $|g\rangle$ and $|i\rangle$ represent real wavefunctions. The matrix elements M_{gi}^σ and M_{ig}^0 are parametrically dependent upon Q , the vibrational coordinates, and are expected to vary weakly with small changes in the equilibrium nuclear coordinates. In order to account for these changes and any consequences which they might bring, it is necessary to expand the matrix elements M^σ and M^0 in a Taylor series around the equilibrium nuclear coordinates which will be represented

by $Q = 0$:

$$\begin{aligned}
 M^\sigma(Q_\xi) &= M^\sigma(Q_\xi=0) + \left(\frac{\partial M^\sigma}{\partial Q_\xi}\right)_{Q_\xi=0} Q_\xi + 0 \\
 &+ \left(\frac{\partial^2 M^\sigma}{\partial Q_\xi^2}\right)_{Q_\xi=0} \frac{Q_\xi^2}{2} + \dots \quad (8)
 \end{aligned}$$

Truncating the series after the first term and using the shorthand notation:

$$M^\sigma(Q_\xi = 0) = \sigma^{(0)}$$

$$\left(\frac{\partial M^\sigma}{\partial Q_\xi}\right)_{Q_\xi=0} = \sigma^{(1)}$$

one has:

$$\sigma(Q_\xi) = \sigma^{(0)} + \sigma^{(1)} Q_\xi \quad (9)$$

Analogously:

$$\rho(Q_\xi) = \rho^{(0)} + \rho^{(1)} Q_\xi$$

It should be noted here that Q_ξ implies summation over all normal modes of vibration. The scattering tensor can now be expressed as a sum of four terms:

$$\begin{aligned}
(\alpha_{\rho\sigma})^{gn,gn'} &= \sum_1 \sum_v \sum_\xi \frac{1}{E_1^v - E^{gn} - \hbar\omega - i\Gamma_1^v} \\
&\times [\sigma^{(0)} \rho^{(0)} \langle n|v \rangle \langle v|n' \rangle \\
&+ \sigma^{(1)} \rho^{(0)} \langle n|Q_\xi|v \rangle \langle v|n' \rangle \\
&+ \sigma^{(0)} \rho^{(1)} \langle n|v \rangle \langle v|Q_\xi|n' \rangle \\
&+ \rho^{(1)} \sigma^{(1)} \langle n|Q_\xi|v \rangle \langle v|Q_\xi|n' \rangle] \quad (10)
\end{aligned}$$

$\sigma^{(1)}$ and $\rho^{(1)}$ can be obtained from perturbation theory:

$$\sigma^{(1)} = \sum_\xi \sum_{s=1} \frac{\langle 1|\mu_\sigma|s \rangle \langle s|(\frac{\partial \hat{H}}{\partial Q_\xi})_0|g \rangle}{E_1^1 - E^s} \quad (11)$$

A similar expression is obtained for $\rho^{(1)}$. Neglecting the $\rho^{(1)} \sigma^{(1)}$ term in the scattering tensor, the summation can be divided up into two parts. The first part will contain the $\rho^{(0)} \sigma^{(0)}$ term and will not vibronically couple any excited electronic states:

$$A_{\rho\sigma} = \sum_1 \sum_v \frac{M_{g1}^\rho M_{1g}^\sigma \langle n|v \rangle \langle v|n' \rangle}{E_1^1 - E^g - \hbar\omega - i\Gamma_1^v} \quad (12)$$

This term is commonly referred to as Albrecht's A term.⁹ Note that the A term contains the product of electronic transition moments and vibrational overlap integrals. For this reason this part is sometimes called the Franck-Condon term.

The second and third terms which contain $\rho^{(1)}_{\sigma^{(0)}}$ and $\rho^{(0)}_{\sigma^{(1)}}$ combine to yield Albrecht's B term:

$$\begin{aligned}
 B_{\rho\sigma} = & \sum_i \sum_{s \neq i} \sum_v \sum_{\xi} \frac{(h_{\xi})_{is}^{(0)}}{(E^i - E^s)(E^{iv} - E^{gn} - \hbar\omega - i\Gamma_{iv})} \\
 & \times [M_{gi}^{\sigma} M_{sg}^{\rho} \langle n|v \rangle \langle v|Q_{\xi}|n' \rangle \\
 & + M_{gi}^{\rho} M_{sg}^{\sigma} \langle n|Q_{\xi}|v \rangle \langle v|n' \rangle] \quad (13)
 \end{aligned}$$

The shorthand notation of Felton and Yu has been adopted:⁸

$$(h_{\xi})_{is}^{(0)} = \langle i | \left(\frac{\partial \hat{H}}{\partial Q_{\xi}} \right)_0 | s \rangle$$

The factor $(h_{\xi})_{is}^{(0)}$ arises from the expansion of the vibronic Hamiltonian in terms of the vibrational coordinates; the B term is also known as the Herzberg-Teller term. It will be smaller than the A term for allowed electronic transitions.

The electronic states of the porphyrins have been discussed in detail by Gouterman.⁵ Since the Soret excitation corresponds to an allowed transition, it is easy to see that the A term will predominate here.

Further considerations show that the Franck-Condon overlap terms will be largest for a_{1g} vibrations, which are polarized. For Soret excitation, this is what is observed: resonance enhancement predominates for completely polarized modes. For excitation occurring in the visible region, if the band is hypothesized to correspond to a forbidden transition, or to a vibronic sideband of that transition, the A and B summations over electronic states can be reduced to two contributing terms, since there are only two major electronic transitions. M_{1g}^{σ} , M_{g1}^{ρ} correspond to the transition dipole for the forbidden transition in both directions, and M_{sg}^{ρ} corresponds to the transition dipole for the Soret transition. An examination of the electronic portions of both A and B reveals that the B term's product of one forbidden and one allowed transition dipole will predominate over the A term's product of two forbidden transition dipoles. However, because the B term contains a vibronic coupling matrix element, $(h_{\xi})_{1s}$, which is less than unity, neither A nor B will predominate overall. Group theoretical considerations show that under these circumstances resonance enhancement should occur for vibrations of symmetry a_{1g} , b_{1g} , a_{2g} , or b_{2g} , all of which

represent in-plane vibrations of the porphyrin ring. Were a feature in the visible region of the spectrum to correspond with a charge transfer between π orbitals on the porphyrin ring and the formyl substituent off the ring, the carbonyl stretching vibration of the formyl group would also be greatly enhanced in the Raman spectrum. Thus a band at 1680 cm^{-1} should appear. If this charge transfer is not involved in the electronic transition, the 1680 cm^{-1} feature would most likely be absent in the Raman spectrum because it is not connected to any of the in-plane porphyrin vibrations and hence should not be resonantly enhanced.

Experimental

Samples of oxidized heme-a were provided courtesy of Dr. G. T. Babcock. The concentrations employed for the resonance Raman investigation ranged from 50-300 mM, in DMSO, as determined from the optical extinctions of the solutions. Samples usually lasted several hours under constant exposure to dye laser radiation. Longer exposure resulted in fluorescence (due to sample degradation) which obscured the Raman signal. Visible spectra were taken before and after each set of Raman data were obtained in order to verify that no sample degradation had occurred, and hence no spurious results were introduced.

The optical spectrum of oxidized heme-a is shown in Figure 4; definitive assignments remain to be made for the two features at 590 and 545 nm. Shown in Figure 5 are the resonance Raman spectra corresponding to excitation at 590 and 545 nm. Asterisks indicate features due to either the solvent or the ligand, N-methyl imidazole. For the Raman spectra obtained at 590 nm, rhodamine 6-G at a power level of approximately 300 mw was used, and for the Raman spectra taken at 545 nm, disodium fluorescein at approximately 150 mw was used. Table 2 lists the major heme-a features and their relative intensities. All are assigned as in-plane porphyrin vibrations. There are no features at 1680 cm^{-1} for either excitation frequency. It should be noted that a repetition of the experiment with methylene chloride instead of DMSO as a solvent, except for minor shifts in the position of the peaks, made no difference.

Results

It is therefore concluded that the band at 590 nm in the visible spectrum corresponds to the forbidden $\pi\text{-}\pi^*$ transition, and it is suggested that the feature at 545 nm corresponds to a vibronic sideband, representing one quanta of vibrational excitation. This interpretation is internally consistent in that 590 and 545 nm lie approximately 1600 cm^{-1} apart; most of the Raman-active

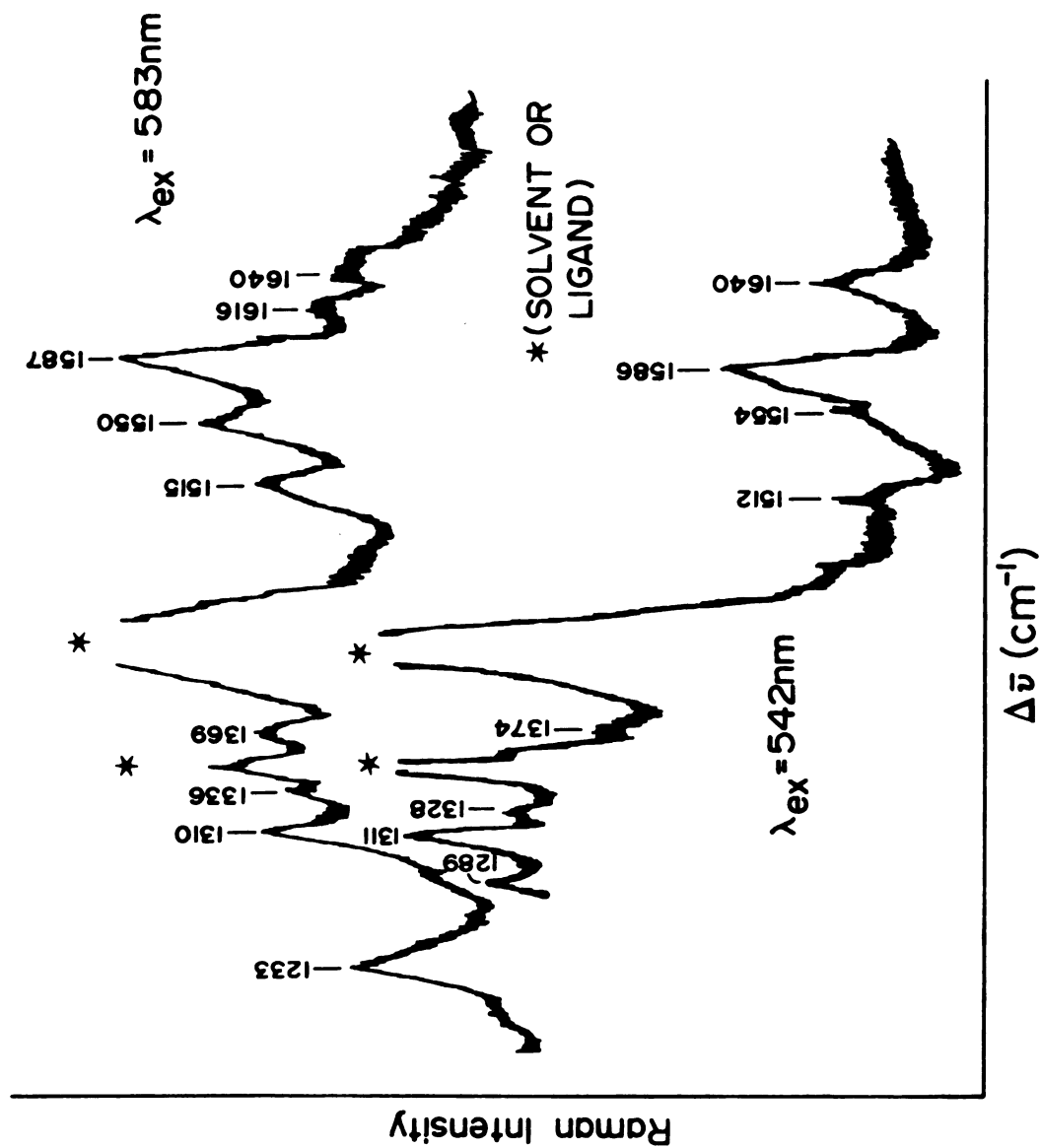


Figure 5. Resonance Raman Spectra of Oxidized Heme-a.

Table 2. Raman Intensities of Oxidized Heme-A.

$\lambda_{\text{ex}}=583 \text{ nm}$ (cm^{-1})	$\lambda_{\text{ex}}=542 \text{ nm}$ $\Delta\bar{\nu}(\text{cm}^{-1})$
1640 w	1640 s
1616 w	
1587 vs	1586 vs
1554 s	1554 m
1515 s	1512 w
1471 w	
1369 w	1374 w
1336 w	1328 w
1310 s	1311 m
1286 vw	1289 m
vs (very strong)	s (strong)
	m (medium)
	w (weak)
vw (very weak)	

heme-a vibrations in the ground state lie in this wave-number range, and their frequencies would be expected to change very little in a low-lying π^* excited state.

Suggestions for Further Work

It is suggested that a more accurate characterization of heme-a would result if more excitation wavelengths, intermediate between 590 and 545 nm were used to obtain resonance Raman spectra. Then definite trends in peak intensity might be observed as excitation frequency is incrementally changed, and further conclusions may be drawn. This can be readily accomplished with the experimental apparatus in its current form.

A complete polarization study would yield additional information as to which resonantly enhanced features in the Raman spectrum under visible excitation arise from Albrecht A-terms and which come from B-terms. This would then facilitate the assignment of the various features shown in Figure 5 to specific modes of vibration.

CHAPTER 4

β -CAROTENE

The class of compounds known as the linear polyenes, to which β -carotene belongs, is characterized by the presence of a chain of alternating single and double carbon-carbon bonds. Various theoretical works have hypothesized the presence of a low-lying, symmetry-forbidden transition to the red of the first allowed absorption peak, which occurs at about 483 nm in β -carotene.¹⁰ It has been suggested that the presence of such a low-lying electronic state may play an active role in the energy transfer from carotenoids to chlorophyll in photosynthesis.¹¹ Hence, it is important to locate and characterize this "phantom state". β -carotene, whose structure is shown in Figure 6 is non-fluorescent and thus two-photon fluorescence (TPF) methods cannot be applied to help locate this state. Because the concentrations necessary to make a two-photon absorption measurement of this state cannot be attained, indirect methods of observation must be sought. One such method is the preresonance Raman excitation profile. Through vibronic coupling, features are seen superimposed on the background of the preresonance portion of the

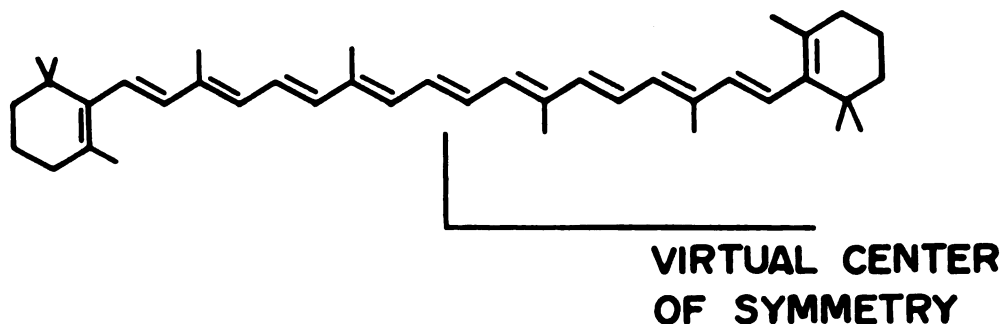


Figure 6. β -Carotene.

excitation profile which may be attributed to these hidden states.

Theory

The theoretical basis for the modulation of the normal preresonance enhancement, due to a symmetry-forbidden transition can be demonstrated simply by expanding the modified scattering tensor used for resonance Raman scattering as shown in Friedman and Hochstrasser.¹² A simplification is made by assuming that the summation contains only two terms. One indicates the low-lying "phantom" state and the other indicates the dipole-allowed state:

$$\alpha_{\rho\sigma} = \sum_i \frac{\langle g | \hat{\mu}_\rho | i \rangle \langle i | \hat{\mu}_\sigma | f \rangle}{E_i - E^g - \hbar\omega - i\Gamma_i}$$

$$= \frac{\alpha_1}{\Delta E_1 - i\Gamma_1} + \frac{\alpha_2}{\Delta E_2 - i\Gamma_2} \quad (14)$$

The Raman scattering intensity due to these states is then proportional to the square of the scattering tensor:

$$I \sim \sum_{\rho\sigma} |(\alpha\rho\sigma)|^2 \quad (15)$$

Here α_1 and α_2 are the geometric mean of the dipole strengths for the transitions connecting the initial and final states via intermediate states one and two, which correspond to the forbidden and allowed electronic states, respectively. Expanding this term leads to the following equation:

$$I \sim \frac{\alpha_1^2}{\Delta E_1^2 + \Gamma_1^2} + \frac{\alpha_2^2}{\Delta E_2^2 + \Gamma_2^2} + \frac{2\alpha_1\alpha_2}{\Delta E_1\Delta E_2 + \Gamma_1\Gamma_2} \quad (16)$$

It has been assumed that all states are real. All imaginary cross terms are neglected. When the excitation energy is close to the energy separation between the "hidden" and ground states, the first term is the resonance term, which is insignificant due to the forbidden nature of α_1 . The second term is a preresonance term due to the nearby allowed electronic transition. The third term, sometimes referred to as the "interference" term, is due to both the forbidden and allowed electronic states and is of significant magnitude due to the cross

product of α_1 and α_2 . Neglecting the resonance term as insignificant, the sum reduces to just two terms

$$I \sim \frac{\alpha_2^2}{\Delta E_2^2 + \Gamma_2} + \frac{2\alpha_1\alpha_2}{\Delta E_1\Delta E_2 + \Gamma_1\Gamma_2} \quad (17)$$

The first term will produce a steadily rising background as the exciting energy approaches the allowed electronic transition. The second term should produce a fluctuation superimposed upon this steadily rising background as the excitation energy becomes coincident with the forbidden transition. This feature would be an indication of a hidden vibronic state.

The experiments of R. J. Thrash,³ which were performed under a similar set of experimental conditions but using a different lasing medium, revealed several features in the preresonance Raman excitation profile in the region between 18200 cm^{-1} and 19000 cm^{-1} . These features were hypothesized to represent interference patterns caused by "hidden" vibronic states.²

The previous study of β -carotene was performed using state-of-the-art instrumentation. Several different dyes were employed, each pushed to the limit of its tuning range. (For example, Thrash obtained barely usable laser power from disodium fluorescein in a region more

the 100 Å to the blue of the limit prescribed by most commercial suppliers.) The Raman spectra were obtained with a single monochromator, which has inferior stray-light rejection compared to the double monochromators normally used. The purpose of the current repetition of that investigation, with an improved laser, and employing a single (different) dye with a broad tuning range as well as a double monochromator, was to assure that instrumental artifacts did not contribute to the previous results.

Experimental

Synthetic β -carotene was obtained from commercial sources (Eastman) and used without further purification. Spectral grade cyclohexane was used also without further purification. The concentration was determined to be 1×10^{-4} M from the Beer's law plot in R. J. Thrash's thesis.³ Coumarin-6, which served as the lasing medium for this experiment, provided a tuning range of 522-552 nm; typical output power ranged from 80-120 mw with a spectral bandwidth of 0.1 nm.

The raman scattering from the sample at $\Delta\nu = 1525 \text{ cm}^{-1}$ (the C=C symmetric stretch) was strong and hence a lower phototube voltage (~ 1600 V) could be used than in the previous experiment; and resulted in an improved signal-to-noise ratio. Monochromator slits were set at

300/600/300 (μm). The electrometer was used at 3×10^{-8} amp full scale deflection.

At each excitation wavelength the ratio of the peak area of the β -carotene band at 1525 cm^{-1} to that of an internal standard solvent band at 1445 cm^{-1} was determined. Measurement of peak areas was made by triangulation. Typical reproducibility was $\pm 5\text{-}10\%$.

Results

The Raman excitation profile thus obtained for β -carotene is shown in Figure 7. Asterisks indicate features reported by Thrash, et al., for comparison the previous excitation profile is reproduced in the inset.

Since this part of the thesis is essentially a replication of Thrash's previous work, a detailed interpretation will not be given. The results found in this study closely resemble and hence tend to confirm those of Thrash; the preresonance Raman excitation profile shows interference effects which are likely due to vibronic states of a "hidden", symmetry-forbidden excited electronic state having its origin near $17,000 \text{ cm}^{-1}$.

Suggestions for Further Work

It has been demonstrated that the exact location of the low-lying forbidden state in linear polyenes is a

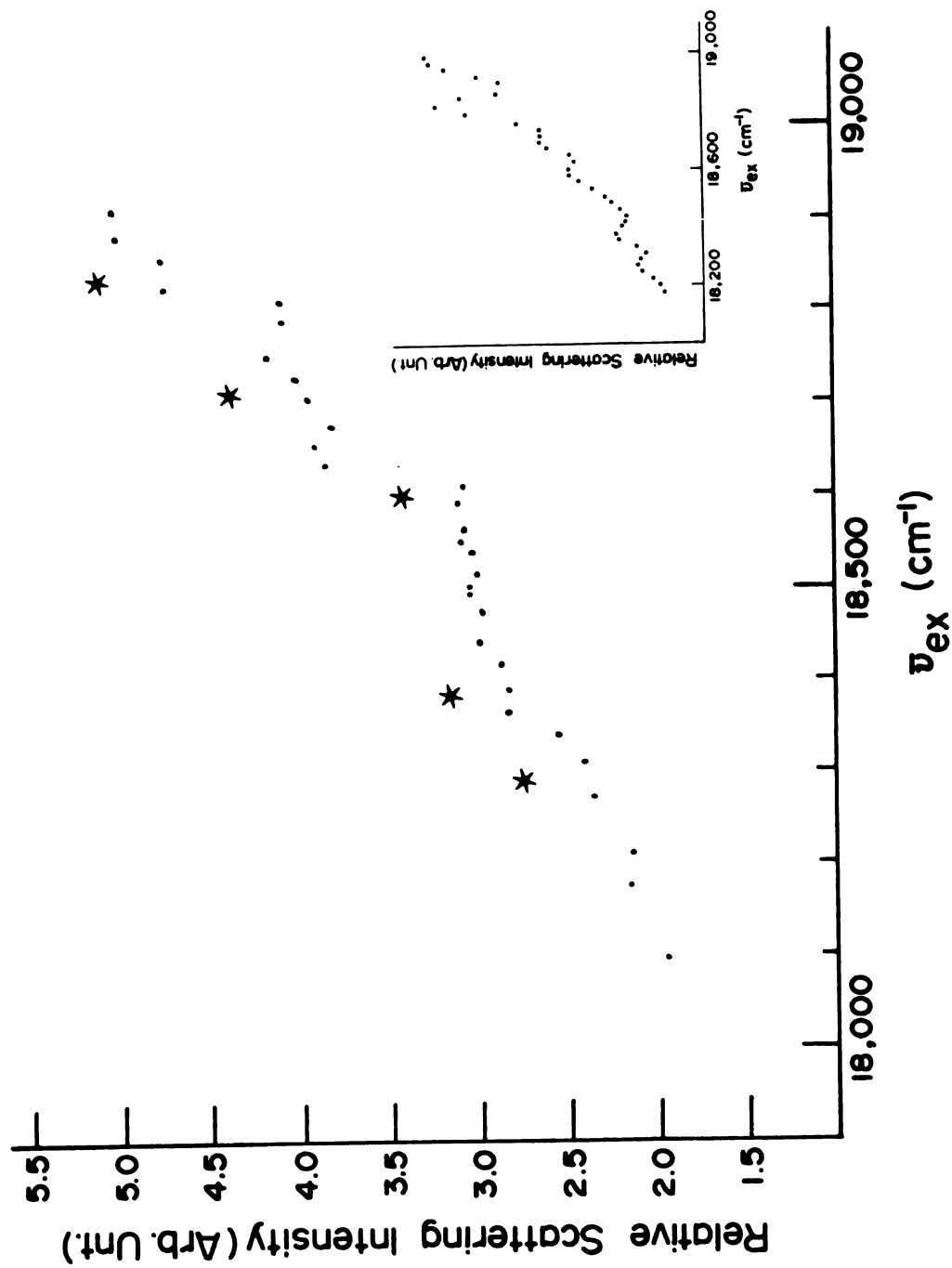


Figure 7. Raman Excitation Profile of β -Carotene in Preresonance Region.

function of the number of double bonds in the polyene.¹³ Quantum mechanical calculations indicate that as the number of double bonds is increased, the low-lying state should drop in energy until it asymptotically reaches a limiting value.¹⁰ This limiting value is predicted to be reached at approximately eleven double bonds. Depending on whether the double bonds in the terminal rings are counted or not, β -carotene has 9 or 11 conjugated double bonds. For comparative purposes, it would be interesting to obtain the preresonance Raman excitation profile of lycopene, a commercially available carotenoid with 11 conjugated double bonds and no terminal rings.

APPENDIX

PREPARATION OF DYE SOLUTIONS

Coumarin 6 - For each liter of final solution, 0.44 grams of the dye should be dissolved in 150 ml of methanol mixed with 150 ml of benzyl alcohol. After the dye is dissolved, which might take 24 hours, 700 ml of ethylene glycol and 3 ml of cyclooctatetraene are added. The entire solution should be filtered by Buchner funnel before being added to the circulator.

Disodium fluorescein - For each liter of final solution. 1.1 gm of the dye should be dissolved in 50 ml of methanol and added directly to 950 ml of ethylene glycol. 4-5 Drops of COT should be added per liter.

Rhodamine-6G - For each liter of solution 0.96 gm of the dye should be dissolved in 50 ml of methanol and added directly to 950 ml of ethylene glycol. Several drops of COT may be added per liter to increase the output power, but this is not necessary and will decrease the lifetime of the dye.

REFERENCES

REFERENCES

1. R. J. Clark, and B. Stewart, Structure and Bonding, 36, 3 (1979).
2. R. J. Thrash, H. L.-B. Fang and G. E. Leroi, J. Chem. Phys. 67, 5930 (1977).
3. R. J. Thrash, Ph.D. Thesis, Michigan State University (1977).
4. T. G. Spiro and T. M. Loehr, in Advances in Infrared and Raman Spectroscopy, 6 ed. R. J. H. Clark and R. E. Hester (Heyden, London, 1975), V.I.
5. M. Gauterman in The Porphyrins, ed. David Dolphin (Academic Press, New York, 1978), V.III.
6. T. Brittain, C. Greenwood, J. Springall, A. J. Thompson, Biochem. J. 173, 411 (1978).
7. F. Adar in The Porphyrins, ed. David Dolphin (Academic Press, New York, 1978), V. III.
8. H. Felton and N. T. Yu, in The Porphyrins, ed. David Dolphin (Academic Press, New York, 1978) V. III.
9. A. Albrecht, J. Chem. Phys., 34, 1476 (1961).
10. P. Tavan, K. Schulten, J. Chem. Phys. 70, 5407 (1979).
11. R. J. Thrash, H. L.-B. Fang and G. E. Leroi, Photochemistry and Photobiology 29, 1049 (1979).
12. J. Friedman and R. M. Hochstrasser, Chem. Phys. Lett. 32, 414 (1975).
13. B. Hudson and B. Kohler, Ann. Rev. Phys. Chem. 25, 437 (1974).

MICHIGAN STATE UNIVERSITY LIBRARIES



3 1293 03061 4840